COMMUN. MATH. SCI.
Vol. 22, No. 4, pp. 977–997

SCALAR AUXILIARY VARIABLE APPROACH IN ITERATIVE MINIMIZATION FORMULATION FOR SADDLE POINT SEARCH*

SHUTING GU†, CHENXI WANG‡, AND ZHEN ZHANG§

Abstract. Saddle points have been extensively investigated in the study of activated process in gradient flow driven by free energy. This paper aims to use the iterative minimization formulation (IMF) coupled with scalar auxiliary variable (SAV) approach to locate the transition states of activated processes in the H^{-1} gradient flow, i.e., index-1 saddle points of the corresponding energy in H^{-1} metric. In each cycle of the IMF, we introduce the SAV approach to minimize the auxiliary functional. A general principle of constructing linear, efficient and robust energy stable schemes for this approach is presented. This new SAV based IMF method improves the efficiency of saddle point search and can be implemented easily for different free energies. By conducting some numerical experiments for the Ginzburg-Landau and the Landau-Brazovskii free energies, the efficient performance of the proposed method is validated.

Keywords. Saddle points; transition states; scalar auxiliary variable; iterative minimization formulation.

AMS subject classifications. 65K05; 82B05.

1. Introduction

Stable points and unstable saddle points of free energies have attracted considerable attention in physics, chemistry, biology and material sciences. Stable points of an energy functional, which correspond to its local minima, manifest themselves as steady states of the gradient flow driven by the corresponding energy. Usually, such gradient flow appears as a time-dependent partial differential equation, which also reflects the actual physical dynamics. For example, the classical Cahn-Hilliard system is the H^{-1} gradient flow driven by the Ginzburg-Landau free energy [2]. As a model for phase separation, its dynamics and steady states have been extensively studied. However, for some free energies, the infrequent hopping between neighboring local minima occurs randomly all the time. Although the occurrences of these events are random, they occur in a fairly certain way of travelling through the transition states. As bottlenecks on paths of activated processes, these transition states belong to a class of saddle points with index-1, which can be defined as the critical points at which the Hessian matrix has one, and only one, negative eigenvalue [40]. Saddle points have been also extensively investigated in the study of activated processes [36, 42, 49, 51]. For instance, in computational chemistry, search for the transition states of the molecular configurations has been widely discussed [35, 36, 50].

In recent years, a large number of numerical methods for searching saddle points have been presented, among which path-finding methods and surface-walking methods are the two most popular classes. The former includes the string method [7, 8, 32, 34] and the nudged elastic band method [20, 23]. The key idea of such methods is

*Received: March 01, 2022; Accepted (in revised form): October 02, 2023. Communicated by Jie Shen.

†College of Big Data and Internet, Shenzhen Technology University, Shenzhen 518118, P.R. China (gushuting@sztu.edu.cn).

‡Corresponding author. International Center for Mathematics, Southern University of Science and Technology (SUSTech), Shenzhen 518055, P.R. China (wangcx2017@mail.sustech.edu.cn).

§Department of Mathematics, International Center for Mathematics, National Center for Applied Mathematics (Shenzhen), Guangdong Provincial Key Laboratory of Computational Science and Material Design, Southern University of Science and Technology (SUSTech), Shenzhen 518055, P.R. China (zhangz@sustech.edu.cn).

to search the so-called minimum energy path (MEP), whose existence is theoretically guaranteed. In this case, the index-1 saddle points are the states along the MEP with locally maximum energies. Surface-walking methods use the unstable direction, e.g., the min-mode direction, to evolve a single state on the potential energy surface. And this class of methods includes the eigenvector following method [6], the quasi-Newton methods [4,41], the activation-relaxation techniques [3,30], the dimer method [14,18,49], the solution landscape method [42], the gentlest ascent dynamics (GAD) [9,25,33] and the iterative minimization formulation (IMF) [12,13,15]. Among these methods, the IMF has the quadratic convergence rate for locating non-degenerate saddle points, which is quite efficient. Moreover, the IMF decomposes the problem of locating unstable saddle points into a series of optimization subproblems, which can be solved in many different ways. Specifically, the IMF contains two-level iterations. The top-level is $x^{(k)} \to x^{(k+1)}$, called "cycle", where superscript k means the k-th cycle. This cycle consists of a "rotation step" whose purpose is to find the softest direction $v^{(k+1)}$ given $x^{(k)}$, and a "translation step" which searches for the best approximation along the softest direction $v^{(k+1)}$ by minimizing $L(y;x^{(k)},v^{(k+1)})$. More precisely, we first do a rotation step, then a translation step; and the translation step can be considered as a second-level iterative procedure to solve the subproblem given $x^{(k)}$ and $v^{(k+1)}$. When solving this subproblem with the fixed pair $(x^{(k)},v^{(k+1)})$, a sequence y_0, y_1, y_2, ... is produced until some stopping tolerance is reached, say, at y_n. And y_n is set as the value of $x^{(k+1)}$. These two-level iterations proceed recursively until a saddle point is located. It is worth noting that the rotation step is indeed a classical eigenvector problem for the min-mode, and thus can be solved by a lot of standard methods, such as the power method [9], the conjugate gradient method [19,21], the LOR [24] and the Lanczos algorithm [3]. In this work, we mainly focus on the translation step and investigate the minimization problem $\min_y L(y;x^{(k)},v^{(k+1)})$.

The flexibilities of the translation step in the IMF immediately provide some opportunities to explore existing methods for local minima search. One of these popular methods is to evolve the gradient flow driven by the functional $L(y;x^{(k)},v^{(k+1)})$ to obtain the minima. Due to the nature of energy dissipation in the gradient flow system, the crucial point becomes how to design schemes preserving the energy stability, which are referred as energy stable schemes. There are a number of different approaches to construct such schemes. Based on a convex splitting technique, unconditionally energy stable methods are proposed in [10,11]. The key point is to split the free energy as the difference of two convex functionals, where the former is treated implicitly and the latter is treated explicitly. Recently, by generalizing the Lagrange multiplier approach [1], Yang et al. [46,52] introduced an auxiliary function for the square root of nonlinear terms in the free energy and constructed a set of energy stable schemes, named invariant energy quadratization (IEQ) methods. And the IEQ approach has been applied in many systems [17,48,53]. Shen et al. [37–39] proposed the scalar auxiliary variable (SAV) methods by introducing an auxiliary scalar variable instead of a function, which enjoy the advantages of the IEQ approach but are more efficient and robust. The SAV approach has attracted a lot of interests [31,45] and has been generalized to develop highly efficient and accurate energy stable schemes for various gradient flow systems [5,22,47].

Recently, based on the IMF and the convex splitting technique, Gu and Zhou [16] developed a general principle of constructing efficient methods for the computation of the transition states of energy functionals, which combined the energy stable schemes with the IMF for the first time. Due to the quadratic convergence rate of the top-level

iteration (cycle) in the IMF, where only a few cycles are needed to reach the desired accuracy in practice, one can expect that an efficient method for the translation step will improve the performance of the whole process. Thus, the benefit of the convex splitting idea in [16], which allows large time step size in minimizing L, improves the overall efficiency of locating the transition states in the IMF. However, while this new method is efficient, it does leave some difficulties to be concerned: (i) The explicit decomposition of the convex splitting form has to be sought case-by-case for specific problems and sometimes it is not so easy to design; (ii) the splitting of many energy functionals leads to nonlinear systems, solving which requires high computational cost at each time step in each cycle in the IMF.

This paper aims to improve the translation step in the IMF by using the SAV approach, which has shown its efficiency and robustness for a large class of gradient flows [39], to solve the gradient flow driven by the objective functional L. Compared with the convex splitting method [16] for the IMF, the SAV approach is easy to be applied to general functionals and always leads to linear systems. The newly proposed method is called the iterative minimization formulation coupled with scalar auxiliary variable approach (IMF-SAV). Specifically, we apply the IMF to locate the transition states of an energy functional in H^{-1} metric. In the translation step of IMF, we employ the SAV approach to develop first- and second-order schemes to solve the H^{-1} gradient flow driven by the auxiliary functional L. Thus, we contribute one more important example of how to construct highly accurate method by using the energy stable schemes for saddle point problems within IMF. In theory, we prove that our first- and second-order schemes preserve the energy decaying property in the discrete sense in each cycle of IMF.

In the numerical experiments, the energy decaying property and the super-linear convergence of the IMF-SAV method are numerically validated. In addition, we apply the IMF-SAV method to numerically locate the transition states for the Ginzburg-Landau and the Landau-Brazovskii free energies very efficiently and accurately. For the nucleation of diblock copolymers in the case of Landau-Brazovskii free energy, we numerically observe that different transition states emerge if we change domain sizes, which clearly shows the size effect of the region.

The paper is organized as follows. We briefly review the IMF and the SAV approach in Section 2. In Section 3, we present the IMF-SAV method for the H^{-1} gradient flows of some typical energy functionals. In Section 4, we validate the accuracy of the proposed schemes in one cycle, and demonstrate the excellent performance of the IMF-SAV method for the saddle point search in the Ginzburg-Landau and the Landau-Bravoskii free energies. Finally, we make the conclusion.

2. Revisiting IMF and SAV

In this section, we review the IMF framework for solving saddle point problems, and the SAV approach to construct unconditionally energy stable schemes. In the next section we will combine these two methods to construct the IMF-SAV method.

2.1. Iterative minimization formulation (IMF). We first review the IMF in [12]. Suppose $\mathcal{M}$ is a function space equipped with a given continuous inner product $\langle\cdot,\cdot\rangle$ and the corresponding norm $\|\cdot\|$. The IMF to search the index-1 saddle points of an energy functional $F(\phi)$ is the following iteration:

$$\begin{cases} v^{(k+1)} = \underset{\|v\|=1}{\operatorname{argmin}} \left\langle v, \delta_\phi^2 F(\phi^{(k)}) v \right\rangle, & (2.1) \\ \phi^{(k+1)} = \underset{\phi}{\operatorname{argmin}} L(\phi; \phi^{(k)}, v^{(k+1)}), & (2.2) \end{cases}$$

where $\delta_\phi^2 F$ is the second order variational derivative of F (corresponding to the metric induced by the given inner product $\langle\cdot,\cdot\rangle$), and the auxiliary objective functional

$$\begin{aligned} L(\phi;\phi^{(k)},v^{(k+1)}) =& (1-\alpha)F(\phi)+\alpha F\left(\phi-\left\langle v^{(k+1)},\phi-\phi^{(k)}\right\rangle v^{(k+1)}\right) \\ & -\beta F\left(\phi^{(k)}+\left\langle v^{(k+1)},\phi-\phi^{(k)}\right\rangle v^{(k+1)}\right), \end{aligned} \tag{2.3}$$

with two parameters α and β satisfying $\alpha+\beta>1$. Two special choices for α and β are: (i) $(\alpha,\beta)=(2,0)$, then $L(\phi;\phi^{(k)},v)=-F(\phi)+2F(\phi-\langle v,\phi-\phi^{(k)}\rangle v)$; (ii) $(\alpha,\beta)=(0,2)$, then $L(\phi;\phi^{(k)},v)=F(\phi)-2F(\phi^{(k)}+\langle v,\phi-\phi^{(k)}\rangle v)$. And the main properties of $L(\phi;\phi^{(k)},v)$ in the case of $\alpha+\beta>1$ are summarised as follows.

THEOREM 2.1 ([12]). *Suppose that ϕ^* is a (non-degenerate) index-1 saddle point of the functional $F(\phi)$, and the auxiliary functional L is defined by (2.3) with $\alpha+\beta>1$, then*

(1) *ϕ^* is a local minimizer of $L(\phi;\phi^*,v)$.*
(2) *There exists a neighborhood $\mathcal{U}$ of ϕ^* such that for any $\phi^{(k)}\in\mathcal{U}$, $L(\phi;\phi^{(k)},v)$ is strictly convex in $\phi\in\mathcal{U}$ and thus has a unique minimum in $\mathcal{U}$.*
(3) *Define the mapping $\Phi:\phi\in\mathcal{U}\to\Phi(\phi)\in\mathcal{U}$ to be the unique local minimizer of $L(\cdot;\phi,v)$ in $\mathcal{U}$ for any $\phi\in\mathcal{U}$. Further assume that $\mathcal{U}$ contains no other stationary point of F except for ϕ^*. Then the mapping Φ has only one fixed point ϕ^*.*
(4) *The iterative scheme $\phi^{(k+1)}=\Phi(\phi^{(k)})$ has the local quadratic convergence rate, i.e., there is a positive constant c such that if the initial starting point $\phi^{(0)}$ is sufficiently close to ϕ^*, then for sufficiently large k, $|\phi^{(k+1)}-\phi^*|\le c|\phi^{(k)}-\phi^*|^2$.*

2.2. Scalar auxiliary variable (SAV). Hereafter, we use $\langle\cdot,\cdot\rangle$ to represent the usual L^2 inner product, and $\frac{\delta}{\delta\phi}$ to represent the variational derivative corresponding to L^2 metric. Consider the typical free energy functional

$$F(\phi)=\frac{1}{2}\langle\phi,\mathcal{L}\phi\rangle+E_1(\phi),$$

where $\mathcal{L}$ is a symmetric nonnegative linear operator (independent of ϕ), and $E_1(\phi)$ is nonlinear and bounded from below, i.e., $E_1(\phi)\ge -C_0$ with $C_0>0$. And the general form of the corresponding gradient flow driven by $F(\phi)$ can be written as

$$\begin{cases} \dfrac{\partial\phi}{\partial t}=\mathcal{G}\mu, & \text{(2.4a)} \\ \mu=\dfrac{\delta F(\phi)}{\delta\phi}=\mathcal{L}\phi+\dfrac{\delta E_1(\phi)}{\delta\phi}, & \text{(2.4b)} \end{cases}$$

supplemented with suitable boundary conditions. Here, $\mathcal{G}$ is a non-positive symmetric operator, such as $\mathcal{G}=-I$ in the L^2 gradient flow and $\mathcal{G}=\Delta$ in the H^{-1} gradient flow, which will be introduced in detail in Section 3.1.

Now, we first introduce an SAV

$$r(t)=\sqrt{E_1(\phi)+C_0},$$

and the gradient flow (2.4) can be rewritten as

$$\begin{cases} \dfrac{\partial \phi}{\partial t} = \mathcal{G}\mu, & (2.5a) \\ \mu = \mathcal{L}\phi + \dfrac{r}{\sqrt{E_1(\phi)+C_0}}\dfrac{\delta E_1(\phi)}{\delta \phi}, & (2.5b) \\ \dfrac{\mathrm{d}r}{\mathrm{d}t} = \dfrac{1}{2\sqrt{E_1(\phi)+C_0}}\left\langle \dfrac{\delta E_1}{\delta \phi}, \dfrac{\partial \phi}{\partial t} \right\rangle. & (2.5c) \end{cases}$$

It can be verified that the equivalent continuous system (2.5) satisfies the energy dissipation law:

$$\frac{\mathrm{d}}{\mathrm{d}t}F(\phi) = \frac{\mathrm{d}}{\mathrm{d}t}\left[\frac{1}{2}\langle \phi, \mathcal{L}\phi\rangle + r^2 - C_0\right] = \langle \mu, \mathcal{G}\mu\rangle \le 0,$$

where the last inequality results from the non-positive symmetric operator $\mathcal{G}$. Then the semi-discrete scheme for the modified system (2.5) is

$$\begin{cases} \dfrac{\phi^{n+1}-\phi^n}{\Delta t} = \mathcal{G}\mu^{n+1}, & (2.6a) \\ \mu^{n+1} = \mathcal{L}\phi^{n+1} + \dfrac{r^{n+1}}{\sqrt{E_1(\phi^n)+C_0}}\dfrac{\delta E_1}{\delta \phi}(\phi^n), & (2.6b) \\ \dfrac{r^{n+1}-r^n}{\Delta t} = \dfrac{1}{2\sqrt{E_1(\phi^n)+C_0}}\left\langle \dfrac{\delta E_1}{\delta \phi}(\phi^n), \dfrac{\phi^{n+1}-\phi^n}{\Delta t} \right\rangle. & (2.6c) \end{cases}$$

The scheme (2.6) is a linear system which can be solved efficiently by decoupling r^{n+1} from ϕ^{n+1} and μ^{n+1}. Furthermore, through straightforward calculations, we can get that the numerical scheme (2.6) also ensures the discrete energy law with respect to the modified energy:

$$\overline{F}(\phi^{n+1}, r^{n+1}) \le \overline{F}(\phi^n, r^n),$$

where $\overline{F}(\eta, s) = \frac{1}{2}\langle \eta, \mathcal{L}\eta\rangle + s^2 - C_0$.

3. The IMF-SAV method

In this section, we first introduce the H^{-1} gradient flow, and limit our discussion to the space embedded with H^{-1} metric. Then we propose efficient and robust methods to search the saddle point of a given free energy.

3.1. H^{-1} gradient flow. A gradient flow is usually determined by a driving free energy and a dissipation mechanism. The gradient flows usually drive the system to its steady states. While for the same energy functional, we have different forms of gradient flows in the different metrics, e.g., the Allen-Cahn and Cahn-Hilliard equation. Indeed, given the Ginzburg-Landau free energy

$$F(\phi) = \int_\Omega \left(\frac{\varepsilon}{2}|\nabla \phi|^2 + \frac{(\phi^2-1)^2}{4\varepsilon}\right)\mathrm{d}\mathbf{x},$$

where ε denotes the interfacial thickness, the corresponding gradient flow in L^2 metric is the classical Allen-Cahn equation,

$$\begin{cases} \dfrac{\partial \phi}{\partial t} = -\dfrac{\delta F}{\delta \phi} = -\mu, & (3.1a) \\ \mu = -\varepsilon\Delta\phi + \dfrac{\phi(\phi^2-1)}{\varepsilon}. & (3.1b) \end{cases}$$

If we consider $\frac{\delta F}{\delta \phi}$ as the gradient of F, the gradient flow (3.1) can be viewed as a "normal" steepest descent dynamics. Next, we will consider the H^{-1} gradient flow. We first give the inner product and norm in the H^{-1} metric,

$$\langle \phi, \psi \rangle_{H^{-1}} = \left\langle (-\Delta)^{-1}\phi, \psi \right\rangle, \qquad \|\phi\|^2_{H^{-1}} = \langle \phi, \phi \rangle_{H^{-1}}. \tag{3.2}$$

Then, the first order variational derivative between the H^{-1} metric and the L^2 metric can be linked as follows:

$$\left.\frac{\delta F}{\delta \phi}\right|_{H^{-1}} = -\Delta \frac{\delta F}{\delta \phi}. \tag{3.3}$$

Hence, we have the H^{-1} gradient flow driven by the Ginzburg-Landau free energy $F(\phi)$ as follows

$$\begin{cases} \dfrac{\partial \phi}{\partial t} = -\left.\dfrac{\delta F}{\delta \phi}\right|_{H^{-1}} = \Delta \dfrac{\delta F}{\delta \phi} = \Delta \mu, & \text{(3.4a)} \\ \mu = -\varepsilon \Delta \phi + \dfrac{\phi(\phi^2 - 1)}{\varepsilon}, & \text{(3.4b)} \end{cases}$$

which is known as the Cahn-Hilliard equation. It is obvious that (3.4) has the property of mass conservation: $\int_\Omega \phi(\mathbf{x}, t)\mathrm{d}\mathbf{x} \equiv \int_\Omega \phi(\mathbf{x}, 0)\mathrm{d}\mathbf{x}$, $\forall t > 0$.

In the next subsection, we will discuss the saddle point problems of given free energy $F(\phi)$ in H^{-1} metric.

3.2. IMF in H^{-1} metric. The IMF in H^{-1} metric can be written as

$$\begin{cases} v^{(k+1)} = \underset{\|v\|_{H^{-1}}=1}{\operatorname{argmin}} \left\langle v, \widetilde{\mathbf{H}}(\phi^{(k)}) v \right\rangle_{H^{-1}}, & \text{(3.5)} \\ \phi^{(k+1)} = \underset{\int_\Omega \phi \mathrm{d}\mathbf{x} = m}{\operatorname{argmin}} L(\phi; \phi^{(k)}, v^{(k+1)}), & \text{(3.6)} \end{cases}$$

where the Hessian matrix $\widetilde{\mathbf{H}}$ is the second order variational derivative of $F(\phi)$ in H^{-1} metric, $m = \int_\Omega \phi(\mathbf{x}, 0)\mathrm{d}\mathbf{x}$ is the initial total mass of ϕ, and the auxiliary functional

$$\begin{aligned} L(\phi; \phi^{(k)}, v^{(k+1)}) =& (1-\alpha)F(\phi) + \alpha F\left(\phi - \left\langle v^{(k+1)}, \phi - \phi^{(k)} \right\rangle_{H^{-1}} v^{(k+1)}\right) \\ & - \beta F\left(\phi^{(k)} + \left\langle v^{(k+1)}, \phi - \phi^{(k)} \right\rangle_{H^{-1}} v^{(k+1)}\right), \end{aligned} \tag{3.7}$$

with the inner product $\langle \cdot, \cdot \rangle_{H^{-1}}$ defined in (3.2). Without loss of generality, we take $\alpha = 0$, $\beta = 2$, and for other choices of α, β satisfying $\alpha + \beta > 1$, similar operations can be performed. Then

$$L(\phi) = F(\phi) - 2F(\hat{\phi}), \tag{3.8}$$

with

$$\hat{\phi} = \phi^{(k)} + \left\langle v^{(k+1)}, \phi - \phi^{(k)} \right\rangle_{H^{-1}} v^{(k+1)}. \tag{3.9}$$

Moreover, the variational derivatives between the H^{-1} metric and the L^2 metric can be linked as follows:

$$\left.\frac{\delta F}{\delta \phi}\right|_{H^{-1}} = -\Delta \frac{\delta F}{\delta \phi}, \qquad \widetilde{\mathbf{H}} := \left.\frac{\delta^2 F}{\delta \phi^2}\right|_{H^{-1}} = -\Delta \frac{\delta^2 F}{\delta \phi^2}. \tag{3.10}$$

As mentioned in Section 3.1, ϕ is mass conserved in H^{-1} metric, i.e., $\int_\Omega \phi \mathrm{d}\mathbf{x} = m$, thus the softest direction $v^{(k+1)}$ obtained from the rotation step (3.5) must satisfy $\int_\Omega v^{(k+1)} \mathrm{d}\mathbf{x} = 0$. In consequence, the eigenvalue problem (3.5) can be rewritten as

$$\begin{cases} \widetilde{\mathbf{H}}(\phi)\psi = \lambda\psi, & (3.11a) \\ \displaystyle\int_\Omega \psi \mathrm{d}\mathbf{x} = 0, & (3.11b) \end{cases}$$

subject to the homogeneous Neumann or periodic boundary conditions. By the representation of the Rayleigh quotient with respect to the H^{-1} metric, the min-mode solves the minimization problem

$$\operatorname*{argmin}_{\int_\Omega \psi \mathrm{d}\mathbf{x}=0} \widetilde{\mathcal{R}}(\psi) := \frac{\left\langle \psi, \widetilde{\mathbf{H}}\psi \right\rangle_{H^{-1}}}{\|\psi\|_{H^{-1}}^2}. \tag{3.12}$$

When the min-mode is obtained, the subproblem (3.6) can be solved by evolving the gradient flow in H^{-1} metric,

$$\frac{\partial \phi}{\partial t} = \Delta \frac{\delta L}{\delta \phi}(\phi), \tag{3.13}$$

subject to either periodic boundary conditions or homogeneous Neumann boundary conditions, where $L(\phi)$ is defined in (3.8). By solving (3.12) and (3.13) recursively, one can get the index-1 saddle point of $F(\phi)$ in H^{-1} metric. Next, we will show how to efficiently solve this gradient flow system (3.13).

3.3. SAV approach to minimize auxiliary functional L. In this part, we present how to use the SAV approach to construct unconditionally energy stable schemes for (3.13). Suppose that the free energy $F(\phi)$ can be split as $F(\phi) = \frac{1}{2}\langle \phi, \mathcal{L}\phi \rangle + F_n(\phi)$, where $\mathcal{L}$ is a symmetric nonnegative linear operator and $F_n(\phi)$ is nonlinear. Then, assume that $F(\phi)$ and $F_n(\phi)$ are respectively bounded by $[-\widehat{C}_0, \widehat{C}_1]$ and $[-\widetilde{C}_0, \widetilde{C}_1]$ with $\widehat{C}_0, \widehat{C}_1, \widetilde{C}_0, \widetilde{C}_1 > 0$. Take $C_0 = \max\{\widehat{C}_0, \widetilde{C}_0\}$ and $C_1 = \max\{\widehat{C}_1, \widetilde{C}_1\}$, hence $F(\phi), F_n(\phi) \in [-C_0, C_1]$. Now we have the following decomposition of $L(\phi)$ in (3.8):

$$L(\phi) = \frac{1}{2}\langle \phi, \mathcal{L}\phi \rangle + F_n(\phi) - 2F(\hat{\phi}) := \frac{1}{2}\langle \phi, \mathcal{L}\phi \rangle + L_n(\phi),$$

where $\hat{\phi}$ is defined in (3.9) and $L_n(\phi) = F_n(\phi) - 2F(\hat{\phi}) \in [-C_0 - 2C_1, 2C_0 + C_1]$.

Next, we set $C = C_0 + 2C_1$, and introduce an SAV:

$$r(t) = \sqrt{L_n(\phi) + C}.$$

Then the gradient flow (3.13) can be rewritten as:

$$\begin{cases} \dfrac{\partial \phi}{\partial t} = \Delta \mu, & (3.14a) \\ \mu = \mathcal{L}\phi + \dfrac{r}{\sqrt{L_n(\phi) + C}} \dfrac{\delta L_n}{\delta \phi}(\phi), & (3.14b) \\ \dfrac{\mathrm{d}r}{\mathrm{d}t} = \dfrac{1}{2\sqrt{L_n(\phi) + C}} \left\langle \dfrac{\delta L_n}{\delta \phi}(\phi), \dfrac{\partial \phi}{\partial t} \right\rangle, & (3.14c) \end{cases}$$

subject to either periodic boundary conditions or homogeneous Neumann boundary conditions. Taking inner product of the equations (3.14a), (3.14b) and (3.14c) with $\mu, \partial_t \phi$ and $2r$ respectively and summing up the results, we can obtain the energy dissipation law:

$$\begin{aligned}\frac{\mathrm{d}L}{\mathrm{d}t} &= \left\langle \mathcal{L}\phi, \frac{\partial \phi}{\partial t} \right\rangle + \left\langle 2r, \frac{\mathrm{d}r}{\mathrm{d}t} \right\rangle \\ &= -\|\nabla \mu\|^2 - \frac{r}{\sqrt{L_n(\phi)+C}} \left\langle \frac{\delta L_n}{\delta \phi}, \frac{\partial \phi}{\partial t} \right\rangle + \frac{r}{\sqrt{L_n(\phi)+C}} \left\langle \frac{\delta L_n}{\delta \phi}, \frac{\partial \phi}{\partial t} \right\rangle \\ &= -\|\nabla \mu\|^2 \\ &\leq 0.\end{aligned}$$

Now, we construct the first-order semi-discrete scheme for the dynamical system (3.14):

$$\begin{cases} \dfrac{\phi^{n+1}-\phi^n}{\Delta t} = \Delta \mu^{n+1}, & \text{(3.15a)} \\ \mu^{n+1} = \mathcal{L}\phi^{n+1} + \dfrac{r^{n+1}}{\sqrt{L_n(\phi^n)+C}} \dfrac{\delta L_n}{\delta \phi}(\phi^n), & \text{(3.15b)} \\ \dfrac{r^{n+1}-r^n}{\Delta t} = \dfrac{1}{2\sqrt{L_n(\phi^n)+C}} \left\langle \dfrac{\delta L_n}{\delta \phi}(\phi^n), \dfrac{\phi^{n+1}-\phi^n}{\Delta t} \right\rangle. & \text{(3.15c)} \end{cases}$$

THEOREM 3.1. *The scheme (3.15) is unconditionally energy stable with respect to the modified energy $\overline{L}(\phi, r)$, i.e.,*

$$\overline{L}(\phi^{n+1}, r^{n+1}) \leq \overline{L}(\phi^n, r^n),$$

where $\overline{L}(\phi, r) = \frac{1}{2}\langle \phi, \mathcal{L}\phi \rangle + r^2 - C$ is the modified energy.

Proof. Taking inner product of (3.15a), (3.15b) and (3.15c) with $\mu^{n+1}, \frac{\phi^{n+1}-\phi^n}{\Delta t}$ and $2r^{n+1}$ respectively and summing up the results, we get

$$-\|\nabla \mu^{n+1}\|^2 = \left\langle \mathcal{L}\phi^{n+1}, \frac{\phi^{n+1}-\phi^n}{\Delta t} \right\rangle + 2r^{n+1} \frac{r^{n+1}-r^n}{\Delta t}. \tag{3.16}$$

By using (3.16) and the inequality

$$(a-b)a \geq \frac{1}{2}\left(|a|^2 - |b|^2\right),$$

we have the discrete energy dissipation law:

$$\begin{aligned}\overline{L}(\phi^{n+1}, r^{n+1}) - \overline{L}(\phi^n, r^n) &= \frac{1}{2}\langle \phi^{n+1}, \mathcal{L}\phi^{n+1} \rangle - \frac{1}{2}\langle \phi^n, \mathcal{L}\phi^n \rangle + (r^{n+1})^2 - (r^n)^2 \\ &\leq \langle \mathcal{L}\phi^{n+1}, \phi^{n+1} - \phi^n \rangle + 2r^{n+1}(r^{n+1} - r^n) \\ &= -\|\nabla \mu^{n+1}\|^2 \\ &\leq 0.\end{aligned}$$

∎

It is worth noting that the scheme (3.15) is easy to implement. Indeed, we can eliminate μ^{n+1} and r^{n+1} from (3.15) to obtain

$$\frac{\phi^{n+1}-\phi^n}{\Delta t}=\Delta\left[\mathcal{L}\phi^{n+1}+\frac{\frac{\delta L_n}{\delta\phi}(\phi^n)}{\sqrt{L_n(\phi^n)+C}}\left(r^n+\left\langle\frac{\frac{\delta L_n}{\delta\phi}(\phi^n)}{2\sqrt{L_n(\phi^n)+C}},(\phi^{n+1}-\phi^n)\right\rangle\right)\right]. \tag{3.17}$$

Denote

$$b^n=\frac{1}{\sqrt{L_n(\phi^n)+C}}\frac{\delta L_n}{\delta\phi}(\phi^n),$$

then Equation (3.17) can be rewritten as

$$(I-\Delta t\Delta\mathcal{L})\phi^{n+1}-\frac{\Delta t}{2}\Delta b^n\left\langle b^n,\phi^{n+1}\right\rangle=\phi^n+\Delta t r^n\Delta b^n-\frac{\Delta t}{2}\left\langle b^n,\phi^n\right\rangle\Delta b^n:=c^n. \tag{3.18}$$

Multiplying (3.18) with $(I-\Delta t\Delta\mathcal{L})^{-1}:=A^{-1}$ and taking inner product with b^n, we have

$$\left\langle b^n,\phi^{n+1}\right\rangle+\frac{\Delta t}{2}\alpha^n\left\langle b^n,\phi^{n+1}\right\rangle=\left\langle b^n,A^{-1}c^n\right\rangle,$$

where $\alpha^n=-\left\langle b^n,A^{-1}\Delta b^n\right\rangle$. Hence,

$$\left\langle b^n,\phi^{n+1}\right\rangle=\frac{\left\langle b^n,A^{-1}c^n\right\rangle}{1+\Delta t\alpha^n/2}. \tag{3.19}$$

To summarize, the scheme (3.15) can be implemented as follows:

(1) Compute b^n and c^n.
(2) Compute $\left\langle b^n,\phi^{n+1}\right\rangle$ from (3.19).
(3) Compute ϕ^{n+1} from (3.18).

REMARK 3.1. We assume that the IMF always has solution for the free energy $F(\phi)$ at least locally. This implies that the auxiliary objective functional $L(\phi)$ is bounded from below. As a result, the boundedness of the functionals $F(\phi)$ and $F_n(\phi)$ holds at least locally.

The unconditionally energy stable schemes can remove constraints on the time step size in the sense of stability. Nonetheless, the larger the step sizes, the larger the numerical errors. In order to use the time step as large as possible while maintaining the required accuracy, highly accurate energy stable schemes are needed. To be more specific, the second-order backward differentiation formula (BDF) scheme for the system (3.14) is proposed as follows:

$$\begin{cases}\dfrac{3\phi^{n+1}-4\phi^n+\phi^{n-1}}{2\Delta t}=\Delta\mu^{n+1}, & \text{(3.20a)}\\ \mu^{n+1}=\mathcal{L}\phi^{n+1}+\dfrac{r^{n+1}}{\sqrt{L_n(\phi^*)+C}}\dfrac{\delta L_n}{\delta\phi}(\phi^*), & \text{(3.20b)}\\ \dfrac{3r^{n+1}-4r^n+r^{n-1}}{2\Delta t}=\dfrac{1}{2\sqrt{L_n(\phi^*)+C}}\left\langle\dfrac{\delta L_n}{\delta\phi}(\phi^*),\dfrac{3\phi^{n+1}-4\phi^n+\phi^{n-1}}{2\Delta t}\right\rangle, & \text{(3.20c)}\end{cases}$$

where $\phi^*=2\phi^n-\phi^{n-1}$.

Similar to the first-order scheme, we have the following theorem.

THEOREM 3.2. *The scheme (3.20) is unconditionally energy stable in the sense that*

$$\widetilde{L}\big[(\phi^{n+1},r^{n+1}),(\phi^n,r^n)\big]\le\widetilde{L}\big[(\phi^n,r^n),(\phi^{n-1},r^{n-1})\big],$$

where the modified discrete energy $\widetilde{L}$ is defined as

$$\widetilde{L}\big[(\phi^{n+1},r^{n+1}),(\phi^n,r^n)\big]:=\frac{1}{4}\Big[\big\langle\phi^{n+1},\mathcal{L}\phi^{n+1}\big\rangle+\big\langle 2\phi^{n+1}-\phi^n,\mathcal{L}(2\phi^{n+1}-\phi^n)\big\rangle\Big]+\frac{1}{2}\Big[(r^{n+1})^2+(2r^{n+1}-r^n)^2\Big].$$

Proof. By taking inner products of $2\Delta t\mu^{n+1}$, $3\phi^{n+1}-4\phi^n+\phi^{n-1}$ and $2\Delta t r^{n+1}$ with (3.20a), (3.20b) and (3.20c) respectively, and using the identity:

$$2\big\langle a^{k+1},3a^{k+1}-4a^k+a^{k-1}\big\rangle=\big|a^{k+1}\big|^2+\big|2a^{k+1}-a^k\big|^2+\big|a^{k+1}-2a^k+a^{k-1}\big|^2-\big|a^k\big|^2-\big|2a^k-a^{k-1}\big|^2,$$

one obtains immediately the desired result. ∎

Moreover, this scheme can be implemented quite efficiently following the similar process in the first-order case.

REMARK 3.2. In this paper, we only prove that the modified energies decrease monotonically in the discrete sense. However, many related works show that the SAV methods also succeed in reducing the original energies, at least numerically [38, 39]. In Section 4.1 we numerically show that both the modified energy and the original energy decay in time in one cycle in the IMF.

REMARK 3.3. The second-order BDF scheme (3.20) can be replaced by the Crank-Nicolson scheme with a similar accuracy and stability result, which is proposed as follows:

$$\begin{cases}\dfrac{\phi^{n+1}-\phi^n}{\Delta t}=\Delta\mu^{n+\frac{1}{2}}, & (3.21a)\\[2mm] \mu^{n+\frac{1}{2}}=\mathcal{L}\dfrac{1}{2}(\phi^{n+1}+\phi^n)+\dfrac{r^{n+1}+r^n}{2\sqrt{L_n(\bar{\phi}^*)+C}}\dfrac{\delta L_n}{\delta\phi}(\bar{\phi}^*), & (3.21b)\\[2mm] \dfrac{r^{n+1}-r^n}{\Delta t}=\dfrac{1}{2\sqrt{L_n(\bar{\phi}^*)+C}}\left\langle\dfrac{\delta L_n}{\delta\phi}(\bar{\phi}^*),\dfrac{\phi^{n+1}-\phi^n}{\Delta t}\right\rangle, & (3.21c)\end{cases}$$

where $\bar{\phi}^*=(3\phi^n-\phi^{n-1})/2$.

4. Numerical examples

In this section, we present several numerical examples to validate the efficiency of the IMF-SAV method, including the one-dimensional Ginzburg-Landau free energy and the two-dimensional and three-dimensional Landau-Brazovskii free energies in four different domains. For the first example, the accuracy of the proposed schemes is checked in one cycle in the IMF. Moreover, all the examples are restricted to the H^{-1} metric. And periodic boundary conditions are considered for all the examples. We use the finite difference method for spatial discretization. The second-order BDF scheme (3.20) is used for temporal discretization and the time step size Δt is fixed at 0.1, except in the accuracy and efficiency test examples. Due to the periodic boundary conditions, we can apply fast Poisson solver to the fully discrete scheme for simplicity.

4.1. Ginzburg-Landau free energy. In this part, we study the transition states of the Ginzburg-Landau free energy $F(\phi)$ on $[0,1]$,

$$F(\phi)=\int_0^1\Big[\frac{\kappa^2}{2}(\frac{\partial\phi}{\partial x})^2+\frac{(\phi^2-1)^2}{4}\Big]\mathrm{d}x, \tag{4.1}$$

where $\phi(x)$ is an order parameter such as the concentration of one of the components in a binary alloy and $\kappa>0$. These saddle points correspond to the "spike-like" stationary solutions, or "canonical nuclei" discussed in [2]. Here, we consider the space-time Gaussian white noise which drives the system bouncing between two local minimum.

The first and the second order variational derivatives of $F(\phi)$ in L^2 metric can be calculated as

$$\begin{aligned}&\frac{\delta F}{\delta\phi}(\phi)=-\kappa^2\partial_x^2\phi+\phi^3-\phi,\\&\frac{\delta^2F}{\delta\phi^2}(\phi)=-\kappa^2\partial_x^2+3\phi^2-1:=\mathbf{H}.\end{aligned}$$

Then, the IMF in H^{-1} metric can be read as

$$\begin{cases}v^{(k+1)}=\underset{\|v\|_{H^{-1}}=1}{\operatorname{argmin}}\left\langle v,\widetilde{\mathbf{H}}(\phi^{(k)})v\right\rangle_{H^{-1}}, & (4.2)\\ \phi^{(k+1)}=\underset{\int_0^1\phi(x)\mathrm{d}x=m}{\operatorname{argmin}}L(\phi;\phi^{(k)},v^{(k+1)}), & (4.3)\end{cases}$$

where $\widetilde{\mathbf{H}}=-\partial_x^2\mathbf{H}$, m is the initial total mass of ϕ and $L(\phi)=F(\phi)-2F(\hat{\phi})$ with

$$\begin{aligned}\hat{\phi}&=\phi^{(k)}+\left\langle v^{(k+1)},\phi-\phi^{(k)}\right\rangle_{H^{-1}}v^{(k+1)}\\&=\phi^{(k)}+\left\langle w^{(k+1)},\phi-\phi^{(k)}\right\rangle v^{(k+1)},\end{aligned} \tag{4.4}$$

where $w^{(k+1)}=(-\partial_x^2)^{-1}v^{(k+1)}$ is the unique solution satisfying the equation $-\partial_x^2w^{(k+1)}=v^{(k+1)}$ and $\int_0^1w^{(k+1)}\mathrm{d}x=0$.

The first subproblem (4.2) is the eigenvalue problem which can be solved by (3.12), and the Rayleigh quotient here is

$$\widetilde{\mathcal{R}}(\psi)=\frac{\langle\psi,\mathbf{H}\psi\rangle_{L^2}}{\|\psi\|_{H^{-1}}^2}=\frac{\int_0^1\kappa^2|\partial_x\psi|^2+(3\phi^2-1)\psi^2\mathrm{d}x}{\int_0^1\psi(\partial_x^2)^{-1}\psi\mathrm{d}x}.$$

After the min-mode is obtained, the minimization problem (4.3) is solved by evolving the following gradient flow

$$\frac{\partial\phi}{\partial t}=\partial_x^2\frac{\delta L(\phi)}{\delta\phi}=\partial_x^2\Big[-\kappa^2\partial_x^2\phi+\phi^3-\phi-2v\left\langle w,-\kappa^2\partial_x^2\hat{\phi}+\hat{\phi}^3-\hat{\phi}\right\rangle\Big], \tag{4.5}$$

where $v=v^{(k+1)}$ refers to the min-mode of (4.2), and $w=w^{(k+1)}$. Note that the flow (4.5) conserves the initial mass $\int_0^1\phi(x,0)\mathrm{d}x$, hence the constraint in (4.3) holds automatically. This result immediately implies that the IMF mapping $\phi^{(k)}\to\phi^{(k+1)}$ conserves the mass in each cycle k. Furthermore, any stationary solution is still stationary if an arbitrary constant is added.

To apply the schemes (3.15) or (3.20) to (4.5), we specify the operator $\mathcal{L}$ and the energy L_n as

$$\mathcal{L}=-\kappa^2\partial_x^2, \qquad L_n=\int_0^1 \frac{(\phi^2-1)^2}{4}-\kappa^2(\frac{\partial\hat{\phi}}{\partial x})^2-\frac{(\hat{\phi}^2-1)^2}{2}\mathrm{d}x.$$

Then, we have

$$\frac{\delta L_n(\phi)}{\delta\phi}=\phi^3-\phi-2v\left\langle w,-\kappa^2\partial_x^2\hat{\phi}+\hat{\phi}^3-\hat{\phi}\right\rangle.$$

In the numerical test, we take $\kappa=0.04$ and the initial mass $m=0.6$. We first validate the accuracy of the proposed schemes to solve the gradient flow (4.5) in one cycle in the IMF. The spatial resolution is fixed to be $\Delta x=10^{-5}$. The numerical solutions are obtained by applying the schemes (3.15) and (3.20) with different time step sizes $\Delta t=1.6\times10^{-3}$, 8×10^{-4}, 4×10^{-4}, 2×10^{-4}, 10^{-4} at time $t=0.01$. The l_2 norm error $e(\Delta t)$ is computed by comparing with reference solution obtained by the scheme (3.20) with $\Delta t=10^{-5}$ and the convergence order is calculated through the formula $\log[e(\Delta t)/e(\Delta t/2)]$. As shown in Table 4.1, the schemes (3.15) and (3.20) achieve the first order and second order accuracy in time, respectively. Here, we remark that the above order of convergence is the rate at which numerical solution of the numerical scheme converges to an exact solution of the gradient flow, rather than the rate of convergence to the minima of L or the saddle point of the problem.

Scheme		Δt=1.6E-3	Δt=8E-4	Δt=4E-4	Δt=2E-4	Δt=1E-4
1st-order	Error	1.57E-2	8.35E-3	4.29E-3	2.16E-3	1.07E-3
	Order	-	0.91	0.96	0.99	1.01
2nd-order	Error	5.13E-4	1.39E-4	3.58E-5	8.89E-6	2.18E-6
	Order	-	1.88	1.96	2.01	2.03

Table 4.1: *Temporal errors and orders of convergence for ϕ at $t=0.01$ with fixed $\Delta x=10^{-5}$ and different temporal step sizes Δt in one cycle in the IMF. The l_2 norm error $e(\Delta t)$ is computed by comparing with the reference solution obtained by the second-order scheme with $\Delta t=10^{-5}$. The order is calculated through the formula* $\log[e(\Delta t)/e(\Delta t/2)]$.

Furthermore, we validate the energy stability in one cycle by taking $\Delta x=0.01$ and $\Delta t=10^{-4}$. Figures 4.1a and 4.1b show that both the modified and original energies decay monotonically in time for both the first-order and second-order schemes.

Next, we test the performance of the IMF-SAV to locate the index-1 saddle point. In this case, we take the mesh grid size $\Delta x=0.01$. Figure 4.1c shows that the saddle point of $F(\phi)$ in H^{-1} metric obtained by the IMF-SAV method is exactly the same as the result obtained by the string method in [51]. Besides, the quadratic convergence rate can also be observed when using the IMF-SAV, see Figure 4.1d. Here, the errors are measured by the force $\|\Delta\delta_\phi F\|_{H^{-1}}$ in each cycle k, where δ_ϕ means $\frac{\delta}{\delta\phi}$.

At last, we compare the performance of the IMF-SAV to that of the IMF coupled with standard gradient descent method (IMF-GD) or classical semi-implicit scheme (IMF-SI), which demonstrates improvements by using the SAV within IMF in terms of numerical stability and efficiency. Moreover, the time steps Δt of these methods are the same across each set of tests. The classical semi-implicit scheme can be constructed as follows,

$$\frac{\phi^{n+1}-\phi^n}{\Delta t}=-\kappa^2\partial_x^4\phi^{n+1}+\partial_x^2(\phi^n)^3-\partial_x^2\phi^n+2\left\langle v,-\kappa^2\partial_x^2\hat{\phi}^n+(\hat{\phi}^n)^3-\hat{\phi}^n\right\rangle v,$$

where $v=v^{(k+1)}$ refers to the min-mode of (4.2).

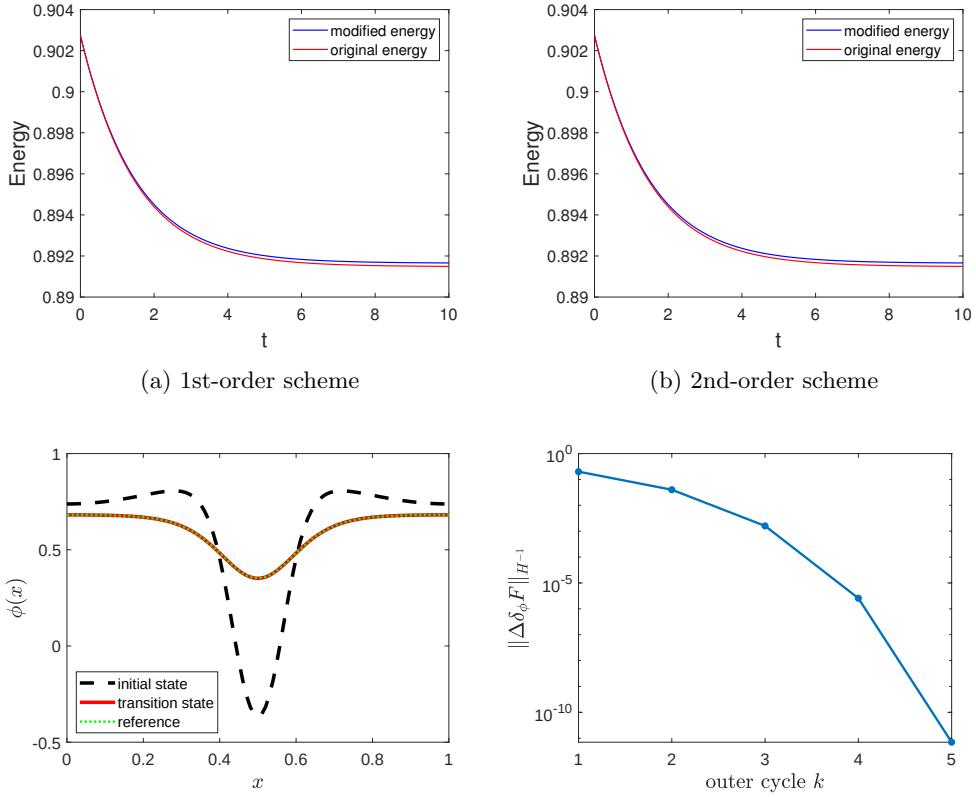

(a) 1st-order scheme (b) 2nd-order scheme

(c) Transition state (d) Convergence rate

Fig. 4.1: *Ginzburg-Landau free energy: (a)-(b) Evolution of original energies (red lines) and modified energies (blue lines) obtained from first-order scheme and second-order scheme in the first cycle of the IMF; (c) initial state (dashed line), transition state obtained by the IMF-SAV (red solid line), reference solution obtained by the string method (green dotted line); (d) the validation of the quadratic convergence rate of the IMF-SAV by plotting the decay of errors, measured by the force* $\|\Delta\delta_\phi F\|_{H^{-1}}$ *in each cycle* k.

We first examine their performance for the subproblem $\operatorname{argmin}_\phi L(\phi;\phi^{(k)},v^{(k+1)})$ in the IMF, where only the inner iteration runs in a fixed cycle. Without loss of generality, we test the first cycle, i.e., $\phi^{(0)}\to\phi^{(1)}$ in the IMF. The number of iterations required to achieve the error tolerances 10^{-4} and 10^{-6} for the three methods is computed, and the errors are measured by the force $\|\delta_\phi L\|_{H^{-1}}$. Table 4.2 shows that the IMF-SAV obviously has much better stability than the others ("∞" in this table means the computational solution diverges). As a result, the larger time step size can be used, which indicates greater efficiency in a single cycle. Then, we will compare the overall efficiency in locating the transition state. In this case, we fix the number of iterations in each cycle and count the number of outer cycles required to attain the prescribed tolerance $\|\delta_\phi F\|_{H^{-1}}\le 10^{-8}$. We can conclude from Table 4.3: If the large step size is adopted, the total number of iterations of the IMF-SAV is much less than that of the other approaches, where the total number is equal to the number of cycles multi-

Δt	The number of iterations					
	$\|\Delta\delta_\phi L\|_{H^{-1}} \le 10^{-4}$			$\|\Delta\delta_\phi L\|_{H^{-1}} \le 10^{-6}$		
	IMF-GD	IMF-SI	IMF-SAV	IMF-GD	IMF-SI	IMF-SAV
1E-4	5276	5118	5162	6067	5911	6011
1E-3	∞	966	986	∞	1298	1263
1E-2	∞	∞	269	∞	∞	350
1E-1	∞	∞	206	∞	∞	256

Table 4.2: *Comparisons of gradient descent method, semi-implicit scheme and SAV for the subproblem* $\operatorname{argmin}_\phi L(\phi;\phi^{(0)},v^{(1)})$ *in the IMF. The integers represent the number of iterations to attain the tolerances* $\|\Delta\delta_\phi L\|_{H^{-1}} \le 10^{-4}$ *or* 10^{-6} *using different step sizes* Δt.

Δt	The number of cycles					
	iter# = 50			iter# = 100		
	IMF-GD	IMF-SI	IMF-SAV	IMF-GD	IMF-SI	IMF-SAV
1E-4	101	96	98	61	56	59
1E-3	∞	33	32	∞	17	18
1E-2	∞	∞	12	∞	∞	8
1E-1	∞	∞	11	∞	∞	7

Table 4.3: *Comparison of the number of outer cycles required for IMF-GD, IMF-SI and IMF-SAV to achieve the tolerance* $\|\Delta\delta_\phi F\|_{H^{-1}} \le 10^{-8}$. *The number of inner iterations is fixed for different temporal step sizes* Δt.

plied by the "iter#" specified in the corresponding columns. This means that the total computational cost of the IMF-SAV can be low and therefore efficient.

4.2. Landau-Brazovskii free energy. In this section, we study the nucleation problem for diblock copolymers between the lamellar and the cylinder phases with a Landau-Brazovskii energy functional for the Cahn-Hilliard dynamics [26, 28, 29, 43, 44]. The Landau-Brazovskii free energy $F(\phi)$ is described as follows

$$F(\phi) = \int_\Omega \frac{\xi^2}{2}[(\Delta+1)\phi(\mathbf{x})]^2 + \Phi(\phi)\ \mathrm{d}\mathbf{x}, \tag{4.6}$$

where $\Phi(\phi) = \frac{\tau}{2}\phi^2 - \frac{\gamma}{3!}\phi^3 + \frac{1}{4!}\phi^4$, and the parameters are chosen as $\tau = -0.15$, $\xi = 1.0$ and $\gamma = 0.25$. With these parameters, the lamellar and the cylinder phases are two equilibrium phases, while the cylinder phase is more stable due to the lower energy. In the following, we focus on the nucleation event from the lamellar phase to the cylinder phase. Here, the first and the second order variational derivatives become

$$\frac{\delta F}{\delta\phi}(\phi) = \xi^2(\Delta+1)^2\phi + \Phi'(\phi),$$
$$\frac{\delta^2 F}{\delta\phi^2}(\phi) = \xi^2(\Delta+1)^2 + \Phi''(\phi) := \mathbf{H},$$

where $\Phi'(\phi) = \tau\phi - \frac{\gamma}{2}\phi^2 + \frac{1}{3!}\phi^3$, and $\Phi''(\phi) = \tau - \gamma\phi + \frac{1}{2}\phi^2$. The corresponding gradient flow becomes

$$\frac{\partial\phi}{\partial t} = \Delta\left[\xi^2(\Delta+1)^2\phi + \Phi'(\phi) - 2v\left\langle w, \xi^2(\Delta+1)^2\hat{\phi} + \Phi'(\hat{\phi})\right\rangle\right],$$

where $v=v^{(k+1)}$, $w=w^{(k+1)}=(-\Delta)^{-1}v^{(k+1)}$ and $\hat{\phi}$ is defined in (4.4). For the scheme (3.20), the operator $\mathcal{L}$ and the energy L_n are specified as

$$\mathcal{L}=\xi^2(\Delta+1)^2, \qquad L_n=\int_\Omega \Phi(\phi)+\frac{\xi^2}{2}[(\Delta+1)\hat{\phi}]^2+\Phi(\hat{\phi})\ \mathrm{d}\mathbf{x}.$$

Then, we have

$$\frac{\delta L_n(\phi)}{\delta\phi}=\Phi'(\phi)-2v\left\langle w,\xi^2(\Delta+1)^2\hat{\phi}+\Phi'(\hat{\phi})\right\rangle_{L^2}.$$

Next, we will discuss the results in two-dimensional and three-dimensional cases, respectively.

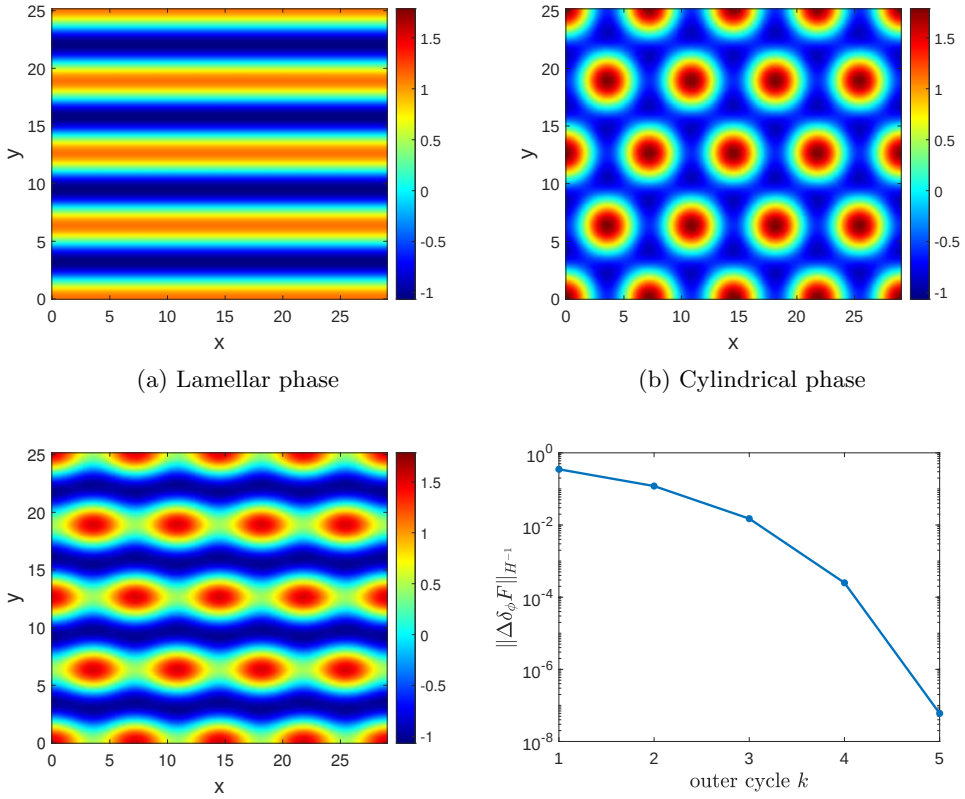

(a) Lamellar phase (b) Cylindrical phase

(c) Transition state (d) Convergence rate

Fig. 4.2: *Small domain* $\Omega=[0,\frac{16\pi}{\sqrt{3}}]\times[0,8\pi]$*: (a)–(b) two stable stationary states of the Landau-Brazovskii free energy in* H^{-1} *metric; (c) the transition state obtained by the IMF-SAV; (d) decay of the error* $\|\Delta\delta_\phi F\|_{H^{-1}}$ *measured by the* H^{-1} *norm of the force in each cycle* k*.*

4.2.1. 2D domain. The two dimensional saddle point problem is numerically solved in three cases with different domain sizes.

Small Domain. We first study the transition state on a small domain $\Omega=[0,\frac{16\pi}{\sqrt{3}}]\times[0,8\pi]$ with $N_x=N_y=60$. Figures 4.2a and 4.2b are the two stable stationary states of

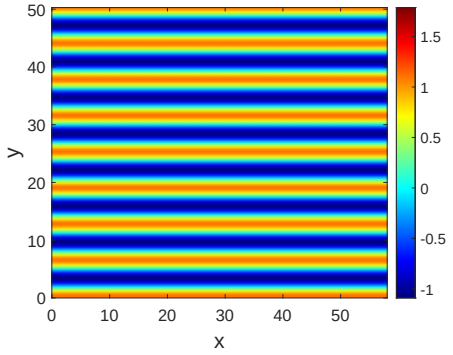

(a) Lamellar phase

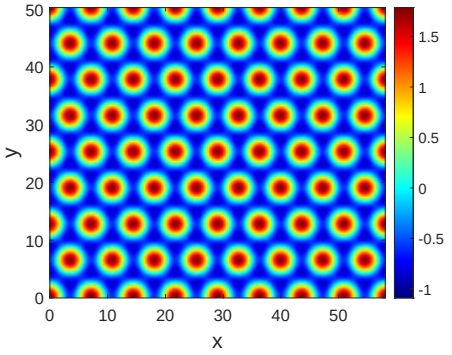

(b) Cylindrical phase

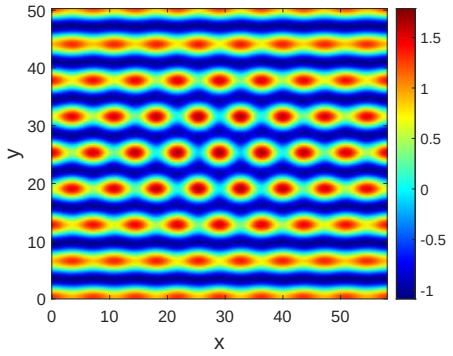

(c) Transition state

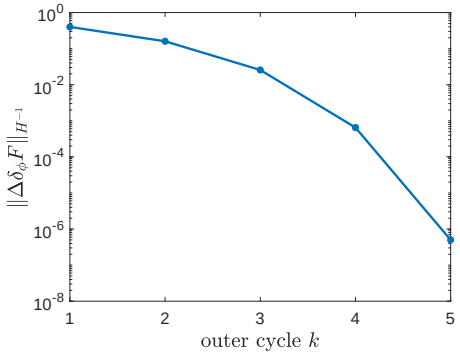

(d) Convergence rate

Fig. 4.3: *Medium domain* $\Omega = [0, \frac{32\pi}{\sqrt{3}}] \times [0, 16\pi]$*: (a)–(b) two stable stationary states of the Landau-Brazovskii free energy; (c) the transition state obtained by the IMF-SAV; (d) decay of the error* $\|\Delta\delta_\phi F\|_{H^{-1}}$ *measured by the* H^{-1} *norm of the force in each cycle* k*.*

the lamellar phase and the cylindrical phase, respectively. The saddle point obtained by the IMF-SAV is shown in Figure 4.2c, and is consistent with the result obtained by the string method in [26]. The quadratic convergence rate can be obtained for the IMF-SAV, which is shown in Figure 4.2d.

Medium Domain. Then we choose the computational domain to be $[0, \frac{32\pi}{\sqrt{3}}] \times [0, 16\pi]$, and the mesh size to be 240×240. The lamellar phase, the cylinder phase, and the saddle point are shown in Figures 4.3a, 4.3b and 4.3c, respectively. Figure 4.3d shows the quadratic convergence rate of the IMF-SAV.

Large Domain. For the last two-dimensional case, we consider a larger domain $\Omega = [0, \frac{64\pi}{\sqrt{3}}] \times [0, 32\pi]$ with mesh size 960×960. Figures 4.4a and 4.4b show the two steady states just like the first two examples. The transition state obtained by the IMF-SAV is shown in Figure 4.4c. In this case, we can see the complete nucleation structure for diblock copolymers, while the nucleation in the small and medium domains are parts of it. The results here are consistent with that in [26]. The quadratic convergence rate of the IMF-SAV can also be obtained, see Figure 4.4d.

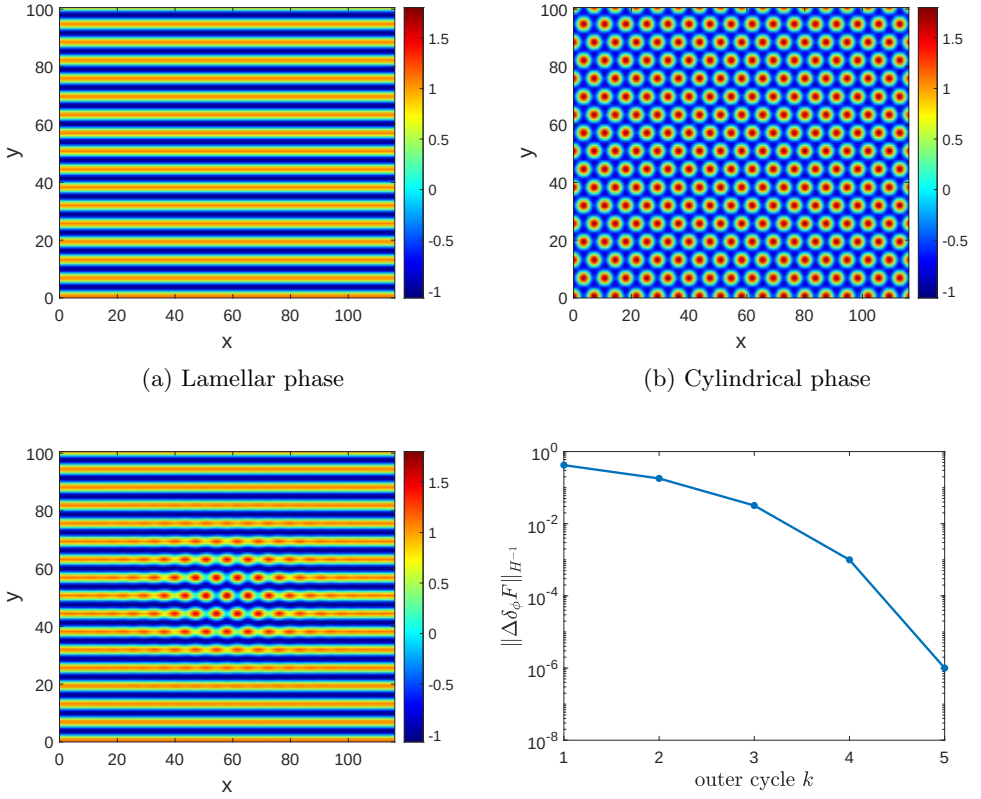

(a) Lamellar phase (b) Cylindrical phase

(c) Transition state (d) Convergence rate

Fig. 4.4: *Large domain* $\Omega = [0, \frac{64\pi}{\sqrt{3}}] \times [0, 32\pi]$*: (a)–(b) two steady states of the Landau-Brazovskii free energy; (c) the transition state obtained by the IMF-SAV; (d) decay of the error* $\|\Delta\delta_\phi F\|_{H^{-1}}$ *measured by the* H^{-1} *norm of the force in each cycle* k*.*

These three two-dimensional examples of the transition states between the lamellar phase and the cylindrical phase show the key features of critical nucleus states in different computational sizes. As the domain size increases, we find that the nucleation occurs significantly in the center of the domain. And the region of significant nucleation seems to have a fixed physical size no matter how large the computational domain is.

4.2.2. 3D domain. Now, we study the transition states of the Landau-Brazovskii free energy on a three-dimensional domain $\Omega = [0, \frac{16\pi}{\sqrt{3}}] \times [0, 8\pi] \times [0, \pi]$, with $N_x = N_y = 60$ and $N_z = 8$. The index-1 saddle point is obtained by the IMF-SAV in Figure 4.5c. From the result, we can see that the transition state here is the analogy of the two-dimensional one being extended in the z-direction, and its projection onto the xy plane corresponds to the two-dimensional transition state in Figure 4.2c. Moreover, Figure 4.5d shows that the IMF-SAV also has the quadratic convergence rate in three-dimensional case. As the free energy landscape is much more complicated in three spatial dimensions, there may be many other transition states that are not captured in our numerical results.

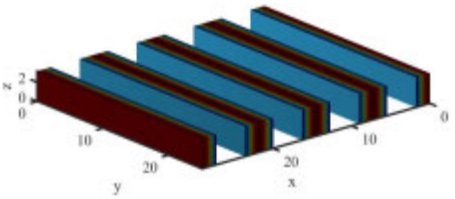

(a) Lamellar phase

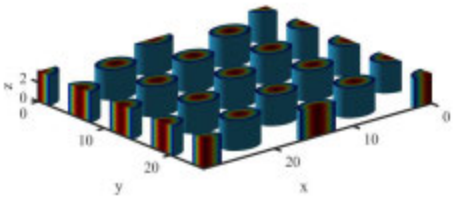

(b) Cylindrical phase

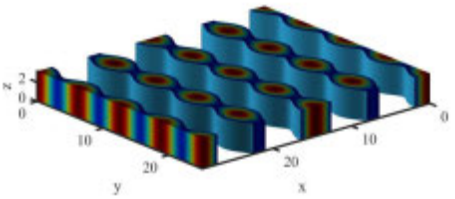

(c) Transition state

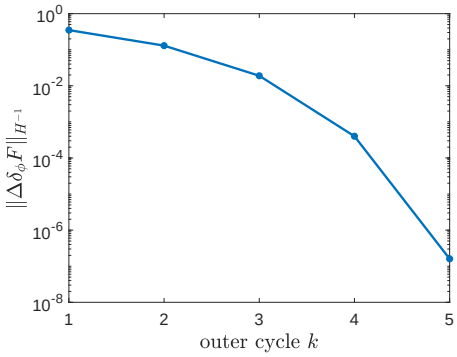

(d) Convergence rate

Fig. 4.5: *3D domain* $\Omega = [0, \frac{16\pi}{\sqrt{3}}] \times [0, 8\pi] \times [0, \pi]$*: (a)–(b) two steady states of the Landau-Brazovskii free energy; (c) the transition state obtained by the IMF-SAV; (d) decay of the error* $\|\Delta\delta_\phi F\|_{H^{-1}}$ *measured by the* H^{-1} *norm of the force in each cycle* k*.*

5. Conclusion

In this paper, we proposed the IMF-SAV method to locate the transition state of some free energies in the activated process by leveraging both strengths of the IMF and the SAV approach. For a given free energy, we showed how to use the IMF-SAV method to search the index-1 saddle point in H^{-1} metric. It is proved that the schemes for minimizing the auxiliary functional L in the IMF are unconditionally energy stable in each cycle, which means the large time step size is allowed. Besides, the IMF-SAV method is easy to apply to general functionals. In the numerical experiments, by testing the examples of the Ginzburg-Landau and the Landau-Brazovskii free energies, we demonstrated that the IMF-SAV method can improve the efficiency and robustness of the transition-state calculation, since SAV only requires solving linear systems and IMF offers quadratic convergence rate at the top-level iteration. Moreover, our numerical results clearly showed the size effect on the transition states for the Landau-Brazovskii free energy.

In this work, we only propose an improvement in the numerical solution of translation step in the IMF. It can be more efficient if we can also improve the numerical solver

for rotation step by exploiting sophisticated eigenfunction solver with faster convergence rate in the H^{-1} metric space. Moreover, the saddle point problems in some other metric spaces are also interesting, e.g., Wasserstein metric space and Hessian transport metric space [27]. These will be our future concern. For the three-dimensional Landau-Brazovskii model, we only considered a relatively small domain to demonstrate the computational efficiency. With a larger domain, one may expect to see richer physics. This is also left for our future study.

Acknowledgments. The authors gratefully acknowledge many helpful discussions with Xiang Zhou and Ling Lin during the preparation of the paper. The work of Shuting Gu was partially supported by the NSFC grant (No. 11901211) and the Natural Science Foundation of Top Talent of SZTU GDRC202137. The work of Zhen Zhang was partially supported by the NSFC grant (No. 12071207), the Natural Science Foundation of Guangdong Province (2021A1515010359), and the Guangdong Provincial Key Laboratory of Computational Science and Material Design (No. 2019B030301001).

REFERENCES

[1] S. Badia, F. Guillén-González, and J.V. Gutiérrez-Santacreu, *Finite element approximation of nematic liquid crystal flows using a saddle-point structure*, J. Comput. Phys., 230(4):1686–1706, 2011. 1

[2] P.W. Bates and P.C. Fife, *The dynamics of nucleation for the Cahn-Hilliard equation*, SIAM J. Appl. Math., 53(4):990–1008, 1993. 1, 4.1

[3] E. Cances, F. Legoll, M.C. Marinica, K. Minoukadeh, and F. Willaime, *Some improvements of the activation-relaxation technique method for finding transition pathways on potential energy surfaces*, J. Chem. Phys., 130(11):114711, 2009. 1

[4] C.J. Cerjan and W.H. Miller, *On finding transition states*, J. Chem. Phys., 75(6):2800–2806, 1981. 1

[5] Q. Cheng, C. Liu, and J. Shen, *A new Lagrange multiplier approach for gradient flows*, Comput. Meth. Appl. Mech. Engrg., 367:113070, 20, 2020. 1

[6] G.M. Crippen and H.A. Scheraga, *Minimization of polypeptide energy: XI. The method of gentlest ascent*, Arch. Biochem. Biophys., 144(2):462–466, 1971. 1

[7] W. E, W. Ren, and E. Vanden-Eijnden, *String method for the study of rare events*, Phys. Rev. B, 66(5):052301, 2002. 1

[8] W. E, W. Ren, and E. Vanden-Eijnden, *Simplified and improved string method for computing the minimum energy paths in barrier-crossing events*, J. Chem. Phys., 126(16):164103, 2007. 1

[9] W. E and X. Zhou, *The gentlest ascent dynamics*, Nonlinearity, 24(6):1831–1842, 2011. 1

[10] C.M. Elliott and A.M. Stuart, *The global dynamics of discrete semilinear parabolic equations*, SIAM J. Numer. Anal., 30(6):1622–1663, 1993. 1

[11] D.J. Eyre, *Unconditionally gradient stable time marching the Cahn-Hilliard equation*, MRS Online Proc. Libr., 529:39–46, 1998. 1

[12] W. Gao, J. Leng, and X. Zhou, *An iterative minimization formulation for saddle point search*, SIAM J. Numer. Anal., 53(4):1786–1805, 2015. 1, 2.1, 2.1

[13] W. Gao, J. Leng, and X. Zhou, *Iterative minimization algorithm for efficient calculations of transition states*, J. Comput. Phys., 309:69–87, 2016. 1

[14] N. Gould, C. Ortner, and D. Packwood, *A dimer-type saddle search algorithm with preconditioning and linesearch*, Math. Comput., 85(302):2939–2966, 2016. 1

[15] S. Gu, L. Lin, and X. Zhou, *Projection method for saddle points of energy functional in H^{-1} metric*, J. Sci. Comput., 89(1):1–17, 2021. 1

[16] S. Gu and X. Zhou, *Convex splitting method for the calculation of transition states of energy functional*, J. Comput. Phys., 353:417–434, 2018. 1

[17] D. Han, A. Brylev, X. Yang, and Z. Tan, *Numerical analysis of second order, fully discrete energy stable schemes for phase field models of two-phase incompressible flows*, J. Sci. Comput., 70(3):965–989, 2017. 1

[18] G. Henkelman and H. Jónsson, *A dimer method for finding saddle points on high dimensional potential surfaces using only first derivatives*, J. Chem. Phys., 111(15):7010–7022, 1999. 1

[19] G. Henkelman and H. Jónsson, *Theoretical calculations of dissociative adsorption of CH_4 on an $Ir(111)$ surface*, Phys. Rev. Lett., 86(4):664, 2001. 1

[20] G. Henkelman, B.P. Uberuaga, and H. Jónsson, *A climbing image nudged elastic band method for finding saddle points and minimum energy paths*, J. Chem. Phys., 113(22):9901–9904, 2000. 1

[21] A. Heyden, A.T. Bell, and F.J. Keil, *Efficient methods for finding transition states in chemical reactions: Comparison of improved dimer method and partitioned rational function optimization method*, J. Chem. Phys., 123(22):224101, 2005. 1

[22] F. Huang, J. Shen, and Z. Yang, *A highly efficient and accurate new scalar auxiliary variable approach for gradient flows*, SIAM J. Sci. Comput., 42(4):A2514–A2536, 2020. 1

[23] H. Jónsson, G. Mills, and K.W. Jacobsen, *Nudged elastic band method for finding minimum energy paths of transitions*, in B. Berne, G. Ciccoti, and D.F. Coker (eds.), Classical and Quantum Dynamics in Condensed Phase Simulations, World Scientific, 385–404, 1998. 1

[24] J. Leng, W. Gao, C. Shang, and Z. Liu, *Efficient softest mode finding in transition states calculations*, J. Chem. Phys., 138(9):094110, 2013. 1

[25] C. Li, J. Lu, and W. Yang, *Gentlest ascent dynamics for calculating first excited state and exploring energy landscape of Kohn-Sham density functionals*, J. Chem. Phys., 143(22):224110, 2015. 1

[26] T. Li, P. Zhang, and W. Zhang, *Nucleation rate calculation for the phase transition of diblock copolymers under stochastic Cahn-Hilliard dynamics*, Multiscale Model. Simul., 11(1):385–409, 2013. 4.2, 4.2.1

[27] W. Li and L. Ying, *Hessian transport gradient flows*, Res. Math. Sci., 6(4):1–20, 2019. 5

[28] L. Lin, X. Cheng, W. E, A. Shi, and P. Zhang, *A numerical method for the study of nucleation of ordered phases*, J. Comput. Phys., 229(5):1797–1809, 2010. 4.2

[29] K. Lu, H. Wang, J. Lin, W. Chuang, P. Georgopanos, A. Avgeropoulos, A. Shi, and R. Ho, *Self-alignment of cylinder-forming silicon-containing block copolymer films*, Macromolecules, 51(19):7656–7665, 2018. 4.2

[30] N. Mousseau and G.T. Barkema, *Traveling through potential energy landscapes of disordered materials: The activation-relaxation technique*, Phys. Rev. E, 57(2):2419, 1998. 1

[31] Y. Qin, Z. Xu, H. Zhang, and Z. Zhang, *Fully decoupled, linear and unconditionally energy stable schemes for the binary fluid-surfactant model*, Commun. Comput. Phys., 28(4):1389–1414, 2020. 1

[32] W. Ren and E. Vanden-Eijnden, *A climbing string method for saddle point search*, J. Chem. Phys., 138(13):134105, 2013. 1

[33] A. Samanta, M. Chen, T.Q. Yu, M. Tuckerman, and W. E, *Sampling saddle points on a free energy surface*, J. Chem. Phys., 140(16):164109, 2014. 1

[34] A. Samanta and W. E, *Optimization-based string method for finding minimum energy path*, Commun. Comput. Phys., 14(2):265–275, 2013. 1

[35] A. Samanta, M.E. Tuckerman, T.Q. Yu, and W. E, *Microscopic mechanisms of equilibrium melting of a solid*, Science, 346(6210):729–732, 2014. 1

[36] H.B. Schlegel, *Exploring potential energy surfaces for chemical reactions: an overview of some practical methods*, J. Comput. Chem., 24(12):1514–1527, 2003. 1

[37] J. Shen and J. Xu, *Convergence and error analysis for the scalar auxiliary variable (SAV) schemes to gradient flows*, SIAM J. Numer. Anal., 56(5):2895–2912, 2018. 1

[38] J. Shen, J. Xu, and J. Yang, *The scalar auxiliary variable (SAV) approach for gradient flows*, J. Comput. Phys., 353:407–416, 2018. 1, 3.2

[39] J. Shen, J. Xu, and J. Yang, *A new class of efficient and robust energy stable schemes for gradient flows*, SIAM Rev., 61(3):474–506, 2019. 1, 3.2

[40] D. Wales, *Energy Landscapes: Applications to Clusters, Biomolecules and Glasses*, Cambridge University Press, 2003. 1

[41] D.J. Wales, *Finding saddle points for clusters*, J. Chem. Phys., 91(11):7002–7010, 1989. 1

[42] W. Wang, L. Zhang, and P. Zhang, *Modelling and computation of liquid crystals*, Acta Numer., 30:765–851, 2021. 1

[43] R.A. Wickham, A.C. Shi, and Z.G. Wang, *Nucleation of stable cylinders from a metastable lamellar phase in a diblock copolymer melt*, J. Chem. Phys., 118(22):10293–10305, 2003. 4.2

[44] S.M. Wise, C. Wang, and J.S. Lowengrub, *An energy-stable and convergent finite-difference scheme for the phase field crystal equation*, SIAM J. Numer. Anal., 47(3):2269–2288, 2009. 4.2

[45] J. Yang and J. Kim, *An improved scalar auxiliary variable (SAV) approach for the phase-field surfactant model*, Appl. Math. Model., 90:11–29, 2021. 1

[46] X. Yang, *Linear, first and second-order, unconditionally energy stable numerical schemes for the phase field model of homopolymer blends*, J. Comput. Phys., 327:294–316, 2016. 1

[47] X. Yang, *A novel fully-decoupled, second-order and energy stable numerical scheme of the conserved Allen-Cahn type flow-coupled binary surfactant model*, Comput. Meth. Appl. Mech.

Engrg., 373:113502, 2021. 1

[48] X. Yang and L. Ju, *Linear and unconditionally energy stable schemes for the binary fluid-surfactant phase field model*, Comput. Meth. Appl. Mech. Engrg., 318:1005–1029, 2017. 1

[49] J. Yin, L. Zhang, and P. Zhang, *High-index optimization-based shrinking dimer method for finding high-index saddle points*, SIAM J. Sci. Comput., 41(6):A3576–A3595, 2019. 1

[50] L. Zhang, W. Ren, A. Samanta, and Q. Du, *Recent developments in computational modelling of nucleation in phase transformations*, NPJ Comput. Mater., 2(1):1–9, 2016. 1

[51] W. Zhang, T. Li, and P. Zhang, *Numerical study for the nucleation of one-dimensional stochastic Cahn-Hilliard dynamics*, Commun. Math. Sci., 10(4):1105–1132, 2012. 1, 4.1

[52] J. Zhao, Q. Wang, and X. Yang, *Numerical approximations for a phase field dendritic crystal growth model based on the invariant energy quadratization approach*, Int. J. Numer. Meth. Eng., 110(3):279–300, 2017. 1

[53] G. Zhu, J. Kou, S. Sun, J. Yao, and A. Li, *Numerical approximation of a phase-field surfactant model with fluid flow*, J. Sci. Comput., 80(1):223–247, 2019. 1